Lawrence Berkeley Laboratory
UNIVERSITY OF CALIFORNIA

EARTH SCIENCES DIVISION
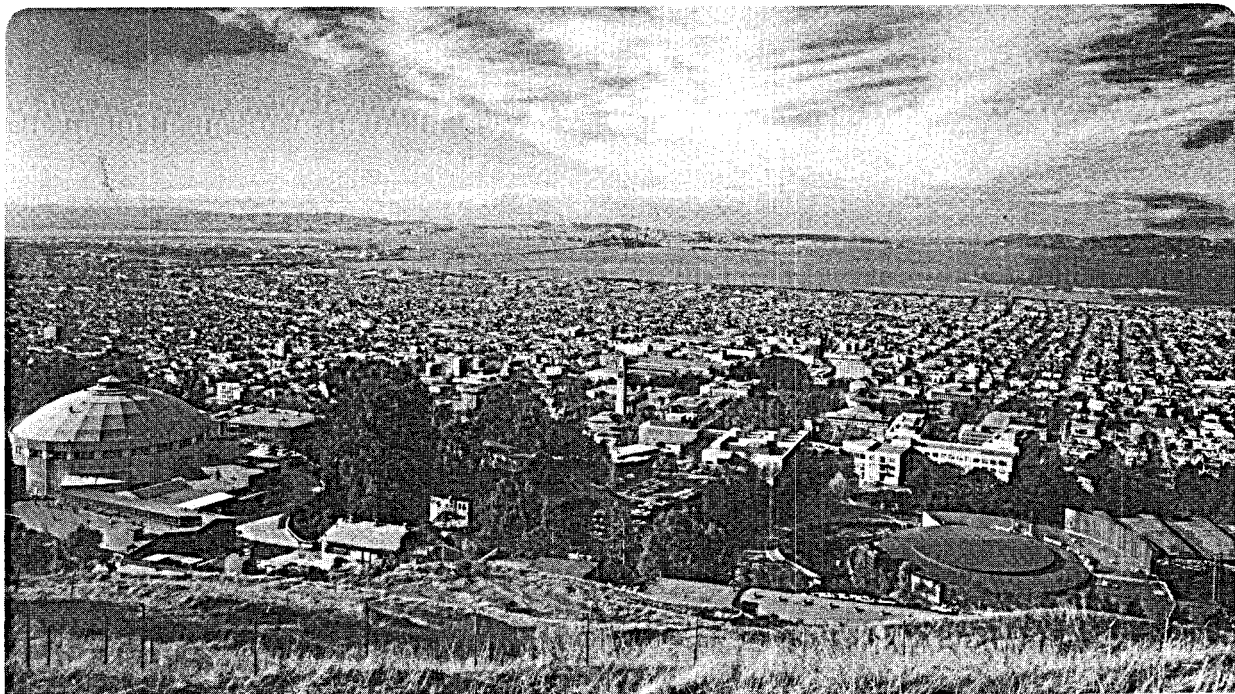
Presented at the SQUID Applications to Geophysics **MASTER**
Workshop, Los Alamos Scientific Laboratory,
Los Alamos, NM, June 2-4, 1980

MAGNETOTELLURIC MEASUREMENTS

John Clarke and N.E. Goldstein

June 1980

DISCLAIMER

DISCLAIMER

Portions of this document may be illegible in electronic image products. Images are produced from the best available original document.

MAGNETOTELLURIC MEASUREMENTS*

John Clarke# and N.E. Goldstein##

ABSTRACT

The ideas of flux quantization and Josephson tunneling are reviewed, and the operation of the dc SQUID as a magnetometer is described. The SQUID currently used for magnetotellurics has a sensitivity of 10^{-14} T $Hz^{-1/2}$, a dynamic range at 10^7 in a 1 Hz bandwidth, a frequency response from 0 to 40 kHz, and a slewing rate of 5×10^{-5} T s^{-1}. Recent improvements in sensitivity are discussed: SQUIDS are rapidly approaching the limit imposed by the uncertainty principle. The essential ideas of magnetotelluric (MT) measurements are outlined, and it is shown how the remote reference method can lead to major reductions in bias errors compared to more conventional schemes. The field techniques of the Berkeley group are described. The practical application of MT requires that amplitude and phase spectra of apparent resistivities be transformed into a geologically useful distribution of subsurface resistivities. In many areas where MT is being applied today, the technique may not provide the information needed because stations are too few and widely spaced, or because we are unable to interpret data influenced by complex 3-D resistivity features. In this paper we examine the results of two surveys, one detailed, the other regional, over the Klamath Basin, Oregon. The detailed survey is able to resolve small (1 km wide) structural features that are missed or add a component of spatial aliasing to the regional data. On the other hand, the regional survey avoids truncation effects that may occur when the survey undersamples an area.

#Department of Physics, University of California, Berkeley, and Materials and Molecular Research Division, Lawrence Berkeley Laboratory, Berkeley, California 94720.

##Earth Sciences Division, Lawrence Berkeley Laboratory, Berkeley, California 94720.

I. INTRODUCTION

During the past five years, the Berkeley group has used dc SQUID magnetometers to perform magnetotelluric (MT) soundings. The purpose of this article is to give a brief overview of this work. We first review a few essential features of superconductivity, describe the operation of the dc SQUID, and then discuss the remote reference technique for magnetotellurics. Brief descriptions of our field techniques follow, and we conclude with a section on the modeling and interpretation of MT data.

II. SUPERCONDUCTIVITY

In a superconductor, electrons are paired together to form Cooper pairs. It is these pairs that are able to carry a supercurrent, and that are responsible for the zero resistance. They also give rise to another very important effect known as flux quantization. Consider a ring of a superconducting material initially above the superconducting transition temperature, and therefore in the normal state. An externally applied magnetic flux threads the ring. The ring is cooled below the transition temperature, and the external magnetic field is switched off. One finds that the initial flux is trapped in the ring by means of a circulating supercurrent that persists indefinitely. However, this flux cannot take on arbitrary values, but is quantized in units of the flux quantum, $\phi_0 = h/2e$, about 2×10^{-15} Wb.

A third highly relevant property of superconductors is Josephson tunneling, illustrated in Figure 1(a). Two superconductors are separated by a thin insulating barrier perhaps 20 to 30 Å thick. Cooper pairs can tunnel through the barrier without dissipation provided the supercurrent they carry is less than a well-defined maximum value, I_0, known as the critical current. A typical plot of current I versus voltage V is shown in Figure 1(b) for a junction shunted by a normal resistor to eliminate hysteresis. At Berkeley, we make such a junction using the following procedure (Figure 1(c)). First, we sputter a strip of Nb, say, 100 μm wide and 2,000 Å thick onto a glass, quartz, or sapphire substrate. We grow an oxide barrier by heating the film in air for typically 12 minutes at 130°C, and complete the junction by depositing a Pb strip

at right angles to the Nb. If, as is usual, we wish to obtain the non-hysteretic I-V characteristic shown in Figure 1(b), we first deposit a diagonal strip of Au that provides a parallel resistance to the junction. We attach current and voltage leads as shown, and measure the I-V characteristic with the junction immersed in liquid helium. The measured characteristic is rather close to that shown in Figure 1(b). For use in the SQUIDS described in the next section, the critical current is typically 2µA, and the shunt resistance is about 1 Ω.
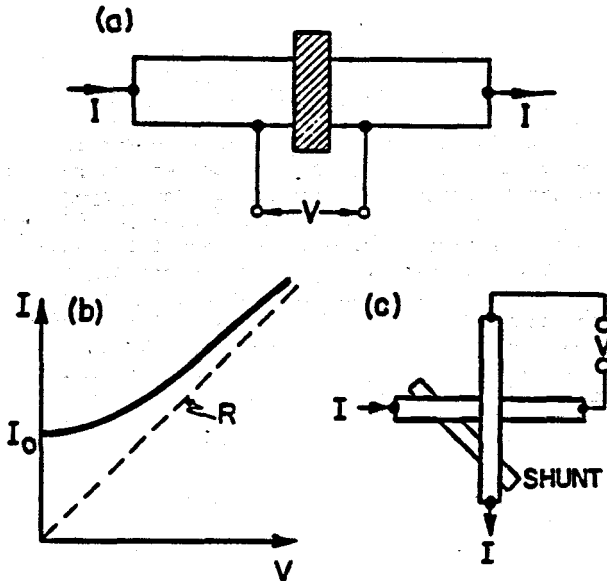
Figure 1 (a) Two superconductors separated by insulating barrier to form a Josephson tunnel junction; (b) current (I) vs. voltage (V) characteristic for a Josephson junction shunted with a resistance, as shown in (c).

III. THE DC SQUID

The dc SQUID neatly incorporates Josephson tunneling and flux quantization. The device consists of a superconducting ring interrupted by two non-hysteretic Josephson junctions (Figure 2(a)). We can measure the I-V characteristic in the usual way. If we change the external magnetic flux threading the ring, we find that the critical current of the SQUID oscillates periodically in the flux, with a period of precisely one flux quantum. The oscillations arise in a way that is analogous to the interference between two beams of light in a two-slit experiment; it is for this reason that we talk about a "quantum interference device." Furthermore, the low-voltage I-V characteristic is also periodic in the applied flux, as indicated in Figure 2(b). Thus, if we bias the SQUID with a constant current, we can see that as the I-V characteristics are modulated by a change in the flux, the voltage across the device also oscillates (Figure 2(c)). Operationally, this is all one needs to know about the SQUID: it is a flux-to-voltage transducer that produces a voltage

change in response to a flux change. The SQUID could thus be used as a digital magnetometer by simply counting the oscillations in voltage as the flux is changed. However, as we shall see presently, in practice one can detect the voltage change that results from a change in flux of much less than ϕ_o, thereby greatly increasing the sensitivity of the device to magnetic field.

Figure 2 (a) dc SQUID, with resistivity shunted junctions; (b) I-V characteristics with fluxes $n\phi_o$ and $(n + 1/2)\phi_o$ threading SQUID; (c) V vs. ϕ.

Figure 3 Practical dc SQUID.

2

Figure 3 shows the type of SQUID developed by Clarke, Goubau and Ketchen (1976) that we have been using for over six years. The device is deposited on a 3-mm-diameter quartz tube. We begi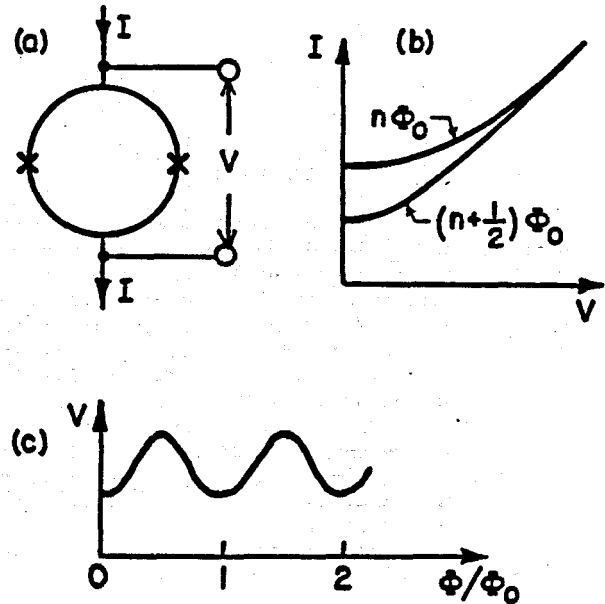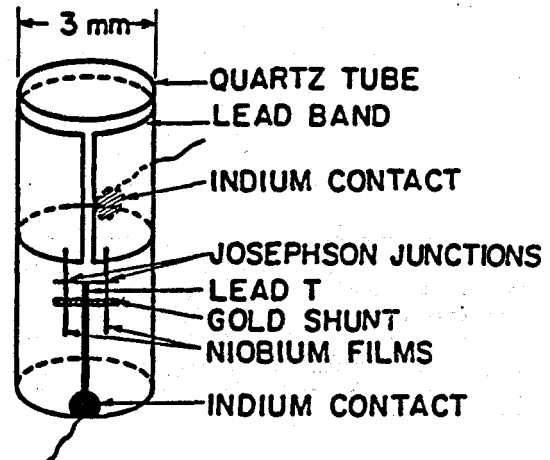n by depositing the Au strips that ultimately serve as shunts, and then deposit a Pb band around the tube. This is followed by two Nb strips that make superconducting contacts to the Pb band. We then oxidize the Nb, and evaporate a Pb "T" to form the two junctions. The SQUID is coated with an insulating layer, and a Pb ground plane (not shown) is evaporated over the slit in the Pb band and the narrow films to reduce the parasitic inductance. Finally, we attach two thin Cu wires with In pellets to enable us to measure the characteristics.

We invariably use the SQUID in a feedback circuit shown schematically in Figure 4. The SQUID is biased with a constant current in the non-zero voltage state. Any change in this voltage is amplified by conventional room-temperature electronics, the output of which is connected via a resistor to a coil placed inside the SQUID. Suppose a small change in flux, $\delta\phi$, is applied to the SQUID. The system responds by inducing a current in the coil that generates an exactly opposing flux, $-\delta\phi$, in the SQUID. The voltage, V_o, produced across the series resistor, R_o, is proportional to $\delta\phi$. Thus, the use of feedback linearizes the response of the SQUID by making it a null detector in which the total flux (applied and feedback) remains constant. In practice, we use a somewhat more complicated system in which we apply a small alternating flux to the SQUID, and amplify the alternating voltage across the device by means of a cooled transformer or resonant circuit. The signal is further amplified by conventional electronics, and lock-in detected before being fed back into the coil.

Figure 5 shows the measured spectral density of the equivalent flux noise of a SQUID enclosed in a Pb shield to eliminate external magnetic interference. In the mid-frequency range, the noise is white, with a magnetic field rms noise of 10^{-14}T Hz$^{-1/2}$. At frequencies below about 2×10^{-2}Hz, the noise scales roughly as $1/f$, where f is the frequency. The high-frequency roll-off is due to a filter placed between the SQUID and the computer used to measure the spectral density; it is not intrinsic to the SQUID or the electronics.
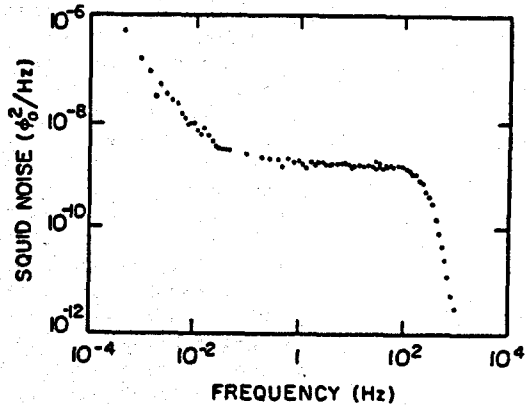
Figure 5 Spectral density of flux noise of SQUID.

Figure 6 shows the long-term drift of the SQUID in a Pb shield in a temperature-regulated He bath. The measured drift was less than 10^{-14}T hr^{-1}.
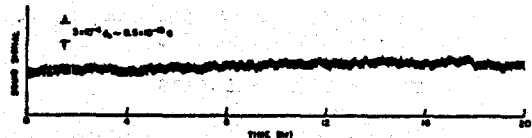
Figure 6 Drift of SQUID output with 0.25 Hz low-pass filter.

The overall specification of the system we use for geophysics is as follows: the dynamic range is about 10^{-7} in a one Hz bandwidth, and the small-signal frequency response is from 0 to about 40 kHz (the upper limit is set entirely by the electronics package - the SQUID itself should operate up to frequencies of one GHz or higher). The slewing rate is about 5×10^{-5} T s^{-1}, and the sensitivity is 10^{-14}T Hz$^{-1/2}$.

Figure 4 Feedback circuit for dc SQUID.

Although the SQUID just described is rather an old design, its performance has been more than adequate for our geophysical measurements. However, new SQUID designs have led to great advances in sensitivity in the last year or so. A convenient measure for the sensitivity of a SQUID is the noise energy per unit bandwidth,

$$\frac{\varepsilon}{1Hz} = \frac{S_\phi}{2L} \quad , \tag{1}$$

where S_ϕ is the spectral density of the equivalent flux noise, and L is the SQUID inductance. The theory of Tesche and Clarke (1977) predicts that ε is proportional to $K(LC)^{1/2}$, where K is the absolute temperature and C is the junction capacitance, which is proportional to the junction area. For practical applications, it is very undesirable to reduce the operating temperature below the boiling point of liquid He, 4.2K, so that one must reduce L and/or C to improve the energy sensitivity. Photolithography and electron-beam lithography have been used very successfully to reduce both the junction areas and the dimensions of SQUIDS. For example, the cylindrical SQUID has an inductance of about one nH, a junction area of about $10^{-2}mm^2$, and a noise energy of about $2\times10^{-30}JHz^{-1}$ at 4.2K. Two recent series of devices with planar geometries have retained an inductance of one nH, but have junction areas of $10^{-4}mm^2$ and $10^{-6}mm^2$, respectively (Koch et al., 1979; Voss et al., 1980a). The measured noise energies were about 2×10^{-31} JHz^{-1} and $2\times10^{-32}JHz^{-1}$, respectively, in accord with the theoretical prediction. At the time of this meeting, the most sensitive SQUID is that described by Voss et al., (1980b) with $\varepsilon/1Hz \sim 2\times10^{-33}Hz \sim 20\,\hbar$ where $\hbar = h/2\pi$ and h is Planck's constant. Recent theoretical calculations (Koch et al., 1981) indicate that the ultimate noise energy is approximately $\hbar$, so that there is still considerable scope for improvement.

The more commonly used cryogenic magnetometer is the commercially available rf SQUID. The rf SQUID is described elsewhere in these proceedings by C.M. Falco and I.K. Schuller. A detailed description of both the dc and rf SQUID can be found in reviews by Clarke (1977 and 1980).

IV. MAGNETOTELLURICS

Magnetotellurics (MT) makes use of ultra-low electromagnetic energy reaching the earth from solar-generated disturbances in the ionosphere (below 1 Hz) and from world-wide electrical thunderstorm activity (above 1 Hz). For a general review of the subject, see, for example, Vozoff (1972). Since the earth is a good electrical conductor compared with the atmosphere, the incident field is reflected, while components of both the magnetic and electric field decay into the ground with a characteristic length equal to the skin depth $\delta \approx 0.5(\rho T)^{1/2}$ in km, where ρ is the electrical resistivity of the earth at the station and T is the period of the oscillation in seconds. The frequency range of interest typically lies between 10^{-4} Hz and 10^2 Hz, and the skin depth at 1 Hz would be on the order of 1 to 5 km. In MT, one measures simultaneously the orthogonal horizontal components of magnetic field, $H_x(t)$

and $H_y(t)$, and the electric field, $E_y(t)$ and $E_x(t)$. From the Fourier transform of these fields, one can compute the impedance tensor, $\underset{\approx}{Z}(\omega)$, defined by:

$$\vec{E}(\omega) = \underset{\approx}{Z}(\omega)\,\vec{H}(\omega). \tag{2}$$

The impedance tensor contains four complex impedance elements $Z_{xx}(\omega)$, $Z_{xy}(\omega)$, $Z_{yx}(\omega)$, and $Z_{yy}(\omega)$. However, the quantity of real physical interest is not so much $Z(\omega)$ but rather $\rho(r)$, the resistivity of the ground as a function of position. In general, it is exceedingly difficult to obtain an accurate picture of $\rho(r)$ from measurements of $\underset{\approx}{Z}(\omega)$, no matter how accurate the latter may be, but it is useful to make some general comments on the problem. However, we note first that one frequently measures a fifth field component, $H_z(t)$, the magnetic field perpendicular to the earth's surface. This quantity enables one to obtain the tipper, $\vec{T}(\omega)$, defined via the relation

$$H_z(\omega) = T_x(\omega)H_x(\omega) + T_y(\omega)H_y(\omega). \tag{3}$$

The simplest modeling situation, and the only one that can be interpreted unambiguously, is the 1-D case in which the conductivity varies with depth, but is independent of position in the x- and y-directions. The H-field is always perpendicular to the E-field, so that $Z_{xx} = Z_{yy} = 0$, and $H_z = 0$, so that $T_x = T_y = 0$. A more complicated situation is the 2-D case in which the conductivity also varies in, for example, the y-direction, but is constant in the x-direction. The x-direction is one of translational invariance, and is called the strike direction in keeping with geological terminology. If we measure the impedance tensor and rotate the axes so that a principal axis lies along the strike, we will again find that $Z_{xx} = Z_{yy} = 0$. Furthermore, $T_x = 0$, but $T_y \neq 0$. Thus a non-zero tipper component provides a direct indication of a change in lateral conductivity. Quite often, one finds that a given survey can be approximated by a 2-D model. However, one may find that the ground is definitely 3-D in which case none of the components of $\underset{\approx}{Z}(\omega)$ or $\vec{T}(\omega)$ is zero, and modeling becomes exceedingly difficult.

The deviation of the real earth from a simple 1-D model motivates the usual method of presenting MT data. The measured fields are related via the expanded form of equation (2):

$$E_x(\omega) = Z_{xx}(\omega)H_x(\omega) + Z_{xy}(\omega)H_y(\omega) \quad , \tag{4}$$

and

$$E_y(\omega) = Z_{yx}(\omega)H_x(\omega) + Z_{yy}(\omega)H_y(\omega) \quad . \tag{5}$$

To obtain any of the impedance elements in the conventional analysis scheme, one multiplies equations (4) and (5) in turn by the complex conjugate fields $H_x^*(\omega)$, $H_y^*(\omega)$, $E_x^*(\omega)$, and $E_y^*(\omega)$, and averages over the resulting auto- and cross-powers to obtain $\overline{H_x(\omega)H_x^*(\omega)}$, $\overline{H_x(\omega)E_y^*(\omega)}$, etc. One then solves a subset of four of these equations to obtain the impedance elements. For example, one method of solution leads to

4

$$Z_{xy}(\omega) = \frac{\overline{E_x H_y^*} \; \overline{|H_x|^2} - \overline{E_x H_x^*} \; \overline{H_x H_y^*}}{\overline{|H_x|^2} \; \overline{|H_y|^2} - \overline{H_x H_y^*} \; \overline{H_y H_x^*}} \qquad [6],$$

with corresponding expressions for the other elements. The usual procedure is to rotate the axes of the impedance tensor analytically until the quantity $|Z_{xx}(\omega)|^2 + |Z_{yy}(\omega)|^2$ is minimized. This defines one of the two directions for which we have the largest translational invariance (the strike). One then ignores the components $Z_{xx}(\omega)$ and $Z_{yy}(\omega)$, thereby assuming that the ground can be adequately represented by a 2-D model. Finally, using Maxwell's equations, one introduces the apparent resistivities in the x- and y-directions

$$\rho_{xy}(\omega) = 0.2 \; |Z_{xy}(\omega)|^2 T \qquad [7]$$

and $\qquad \rho_{yx}(\omega) = 0.2 \; |Z_{yx}(\omega)|^2 T, \qquad [8]$

where T is the period in seconds, ρ_{xy} and ρ_{yx} are in Ωm, and Z_{xy} and Z_{yx} are in $(mV/km)(nT)^{-1}$.

Where the ground can be represented by a 2-D model, we often associate the apparent resistivities in the principal directions (equations (7) and (8)) with either the transverse electric (TE) or transverse magnetic (TM) modes of wave propagation, and these terms are often used in MT nomenclature. The TE mode refers to the electric field parallel to strike, while the TM mode refers to the magnetic field parallel to strike. For example, if x is the strike direction then $\rho_{xy}(\omega)$ is called the TE mode apparent resistivity.

In 1974, Gamble, Goubau, and Clarke began a project to use 3-axis dc SQUID magnetometers for magnetotelluric measurements. This work was undertaken following a suggestion by Profesor H.F. Morrison that the use of more sensitive magnetometers might lead to an improvement in the quality of MT data in bands of low signal strength. A good deal of data was obtained without undue difficulty, but in the subsequent analysis it was found that the apparent resistivities contained very large errors. The source of the error is well-known, and can easily be seen by inspection of equation (6). The denominator contains the autopower $\overline{|H_y(\omega)|^2}$. In fact, all methods of solving equations (4) and (5) for Z_{xy} and Z_{yx} lead to a result with at least one auto-power in the denominator or numerator. Suppose now that $H_y(t)$ actually consists of two components, a "signal" part and a "noise" part:

$$H_y(t) = H_{ys}(t) + H_{yn}(t) . \qquad [9]$$

Computing the auto-power and assuming that the signal and noise parts are uncorrelated, we find

$$\left| \overline{H_y(\omega)} \right|^2 = \left| \overline{H_{ys}(\omega)} \right|^2 + \left| \overline{H_{yn}(\omega)} \right|^2 . \qquad [10]$$

Under certain circumstances, $\overline{|H_{yn}(\omega)|^2}$ can greatly exceed $\overline{|H_{ys}(\omega)|^2}$, thereby "biasing" $Z_{xy}(\omega)$ to a value much lower than its true value. Clearly, no amount of averaging will reduce this error. As a result of this preliminary work, Gamble, Goubau, and Clarke concluded that the source of the noise, although unknown in origin, did not lie in the magnetometer, and began to examine other techniques for overcoming this problem.

After a prolonged investigation, these authors finally tried a method they called the "remote reference technique." The essential idea is to install a second two-axis magnetometer at a site (for example) 5 to 10 km from the primary MT site. Data from the remote site is broadcast to the MT site, and recorded simultaneously with the local data. To analyze these data, we then multiply equations (4) and (5) by the complex conjugates of the remote fields, $H_{xr}^*(\omega)$ and $H_{yr}^*(\omega)$, to obtain four equations that can be solved for the impedance elements. As an example, one finds:

$$Z_{xy}^{(r)}(\omega) = \frac{\overline{E_x H_{yr}^*} \; \overline{H_x H_{xr}^*} - \overline{E_x R_{xr}^*} \; \overline{H_x H_{yr}^*}}{\overline{H_x H_{xr}^*} \; \overline{H_y H_{yr}^*} - \overline{H_x H_{yr}^*} \; \overline{H_y H_{xr}^*}} . \qquad [11]$$

It is immediately evident that equation (11) contains no auto-powers. Furthermore, if the noises in the local fields are uncorrelated with the noises in the reference fields, the noise terms will average to zero, and the impedance elements will be free from bias.

To test the method, which relies critically on the assumptions that the local and remote noises are uncorrelated, an MT station was established at Upper La Gloria in Bear Valley, California, with a second site at Lower La Gloria, roughly 5 km away. All of the data were recorded on tape at Upper La Gloria, and subsequently analyzed. Figure 7 shows the apparent resistivities obtained from one set of data using the remote reference analysis scheme. The apparent resistivities are smooth functions of frequency. To test the effectiveness of the remote reference technique, we re-analyzed the same set of data using the conventional analysis technique (for example, equation (6)). We see in Figure 8 that this technique yielded wild, unphysical swings in the apparent resistivity as a function of frequency. The very considerable improvement that results from the use of the remote reference scheme is clearly demonstrated.
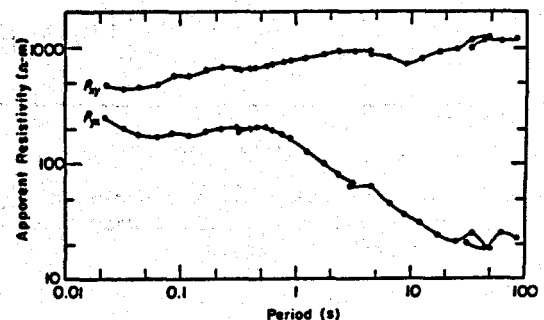

Figure 7. Apparent resistivities obtained from one set of data at Upper La Gloria, using remote reference method.
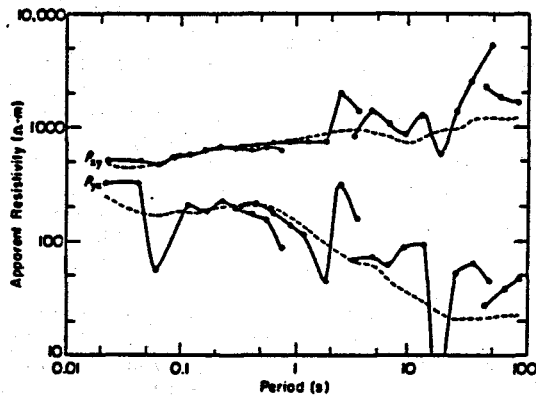
Figure 8 Apparent resistivities obtained from the same set of data as in Fig. 7, using conventional analysis scheme (solid line). Dashed lines represent curves in Fig. 7.

We note that two other benefits result from the use of the remote reference scheme. First, it enables one to place reliable confidence limits on the apparent resistivities. This is essential if one is to perform meaningful modeling. The apparent resistivities of Figure 7 have been replotted in Figure 9 with probable error bars shown. The probable errors can be as low as a few tenths of one percent at high frequencies where many data segments are available. Second, one can re-analyze the data to separate out the "signal" terms from the "noise" terms. In fact, one often finds that the "noise" is higher than the "signal," but, nevertheless, the remote reference scheme enables one to obtain reliable, accurate apparent resistivities.
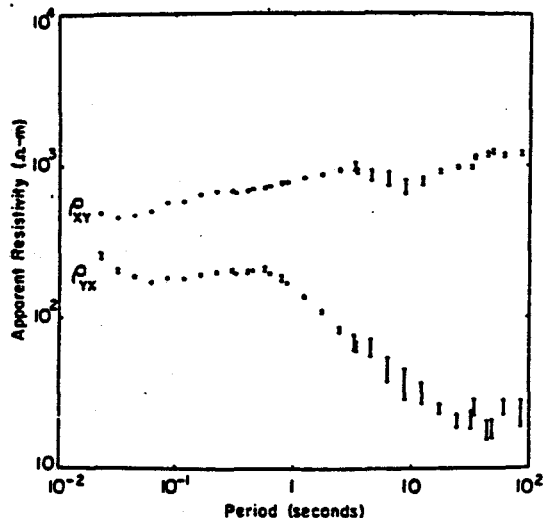

Figure 9 Apparent resistivities shown in Figure 7 replotted with vertical bars representing the probable errors.

V. FIELD TECHNIQUES

.We briefly describe the field techniques that the Berkeley group currently uses. The electrodes for measuring the E-field consist of the usual ceramic pots with a permeable bottom. Each pot contains a saturated solution of $CuSO_4$ in which a Cu electrode is immersed. The electrodes are placed typically 200 m apart, and the voltage between the common electrode and each of the two other electrodes is detected with a low-noise preamplifier. The three SQUIDS are mounted orthogonally in a 5-liter capacity superinsulated fiberglass cryostat. The cryostat uses no liquid nitrogen, and the liquid helium loss rate is approximately 1 liter per day. The cryostat is readily portable and could easily be carried into remote areas on a back-pack frame; it is also very robust. All the magnetometer electronics are mounted on the top of the cryostat; one needs only to connect batteries and a recording system. The magnetometer needs no adjustment in the field. After being switched on, the electronics automatically set the output to zero, and the device is ready to measure the magnetic field fluctuations. We find it necesary to protect the cryostat with a wind- and sun-shield. In fact, wherever possible, we bury the cryostat, particularly in the case of the remote magnetometer, which may be left unattended for days at a time. Incidentally, we now use a 30-liter cryostat for the remote reference, with a hold time of about one month.

The data are recorded in a closed truck. The two E-field signals and the three local H-field signals are connected to the vehicle with cables, while the two remote H-fields are telemetered to the vehicle. After suitable filtering all seven signals are recorded. Typically, below 1 Hz the data are recorded on a digital tape recorder, while above 1 Hz the data are analyzed by a LSI-11 microprocessor that computes all the required auto- and cross-power spectra. At the completion of any set of data, we can print out the essential information to assess its quality.

VI. INTERPRETATION OF FIELD MEASUREMENTS

As explained above, MT workers are now capable of making MT measurements with a high degree of accuracy, and of obtaining impedance estimates with good statistical reliability, even in the frequency band of low signal strength. The major task before the geophysicist is to transform the measured impedances into geologically useful information. This involves finding a half-space distribution of resistivities that fits the complex impedances over the survey area.

Initially, this was not a particularly formidable problem because most early surveys were conducted at sites in topographically flat sedimentary basins (Cagnaird, 1953) where the apparent resistivity, $\rho_a(\omega)$, was invariant with respect to orientation of the horizontal coordinates. Then, as is yet the practice in some areas of the world, a single induction-coil magnetometer and a single pair of electrodes were used to obtain "scalar" impedance estimates which were interpreted mainly by fitting $\rho_a(\omega)$ to sets of layered-earth curves.

However, scalar surveys are rarely performed in the United States today, unless there is a priori evidence that the area is structurally one-dimensional. For those rare cases, interpretation is simplified by use of several direct inversion techniques; e.g. Weidelt (1972), Bostick (1977), and Oldenburg (1979).

The need to apply the MT technique to areas of complex geology has prompted the measurement of the impedance tensor, $\underline{Z}(\omega)$, (see Section IV) and hence the requirement to develop numerical techniques for 2- and 3-D forward solutions to the electromagnetic scattering problem. Several forward solutions to the 2-D problem are in general use, such as variations of the network analogy (Swift, 1971), integral equation (Lee and Morrison, 1980), and finite element-finite difference approaches (Ryu, 1971). Computation costs are in the range of $10 to $50 per model, depending on model complexity and machine used, and various programs are routinely used by the LBL and others. Often we begin an interpretation by employing a 1-D inversion on part of the data to pin down a few parameters, switching over as soon as possible to a trial and error forward 2-D solution. We might then seek to optimize the fit by means of an automatic interative 2-D direct inversion (Jupp and Vozoff, 1977) once a reasonable model has been found that seems consistent with all known data. Recently, there has been an interest in approximate non-iterative direct 2-D inversions (Coen, 1980). Whether this approach will be successful has been questioned because of problems related to (a) non-uniqueness, (b) geological noise, (c) the need for close-spaced stations, and (d) the large amount of computer time required. Also, as the technique involves non-linear transformations, good initial estimates of model parameters are needed and these are usually difficult to obtain unless sufficient geological and geophysical data are available.

Although 2-D interpretations are sometimes adequate to interpret a line of stations perpendicular to geologic strike, we discover that as the station array is expanded in the strike direction, a 3-D interpretation is invariably needed. For this there exists an assortment of forward 3-D solutions based on the integral equation method (Hohmann and Ting, 1978), the finite element method (Pridmore, 1978), or a hybrid of the two (Lee et al., 1981). Regardless of algorithm, the cost of 3-D modeling remains high and these codes are not exercised much beyond the point of testing them on simple models involving a few frequencies. Consequently we do not yet have an efficient means for making topographic corrections, and MT stations located on or near mountains and ridges will yield data degraded by what is equivalent to geologic noise.

While efforts continue for finding improved schemes to reduce the cost of 3-D forward model calculations, the application of MT to more challenging geological problems has identified several other practical problems that were less evident in the past. One general problem centers on the difficulty of obtaining a sufficient number of stations upon which to base an interpretation.

This problem manifests itself in various ways; one fairly common one occurs for surveys in areas of limited access to vehicles. One means for mitigating the access problem has been the use of the telluric-magnetotelluric (T-MT) technique (Hermance, et al., 1975; Hermance and Thayer, 1976). In this technique, a five-component base station is installed at a convenient location, while an array of telluric (E_x, E_y only) stations, with suitable radio telemetry, is placed around it (Figure 10). Magnetotelluric analyses are performed using a common magnetic field; i.e., assuming a uniform magnetic field over the survey area. Although magnetic fields can be uniform over large distances, 30 to 50 km, this is not true everywhere; e.g., in coastal areas or areas where strong lateral contrasts exist in surface rocks.
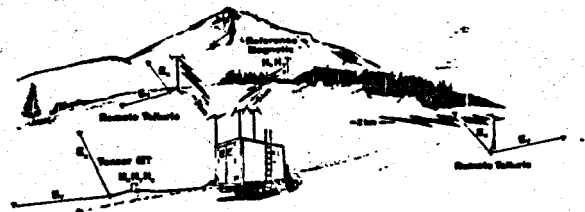

Figure 10. Magnetotelluric sensor array using remote telluric and magnetic stations.

The problem of obtaining adequate station density also arises in areas where subsurface geological information is insufficient for survey planning purposes. If the station separations are kept small, survey time and costs will escalate at an unacceptable rate. For this reason, it is more likely that the geophysicist will make the station density as low as he feels is safe, but, nevertheless, risking the dual dangers of (a) loss of important information due to truncation effects or gaps or (b) error introduced by spatial aliasing. The general problem of undersampling is a major source of concern that is most likely to arise because, for reasons of cost, access, or poor geological information, stations are too far apart relative to the lateral dimensions of subsurface resistivity changes. It may also arise whenever inadequate information is obtained; e.g., (a) at stations located where 3-D topographic corrections are important, (b) where the T-MT method does not provide enough information at the telluric-only stations to discriminate the geologic strike direction, or (c) where stations may not have been located far enough away from the primary area of interest to provide the regional "background."

To illustrate the interpretative problems and inaccuracies that derive from undersampling, we present the results from two surveys conducted in the Klamath Basin in southern Oregon (Stark, et al., 1979 and 1980). The area was subjected to post-Miocene crustal extension resulting in a complex graben structure, characterized by numerous N40°W

normal faults, intermittent volcanism, and pro-
nounced linear physiographic features typical of
the Basin and Range province. The first survey
was a detailed T-MT survey performed by Geonomics,
Inc. in the Swan Lake-Meadow Lake area, 10 km NE
of the city of Klamath Falls. A line of stations
(Line A-A') was placed at nearly right angle to
the Basin and Range faults; the station spacing was
approximately 2 km (Figure 11). Three of the nine
stations, those without a letter designation, were
complete five-component stations. The other six
(4A, 2A, 2C, 6A, 8A, and 8B) were telluric-only
stations, for which the simultaneous magnetic
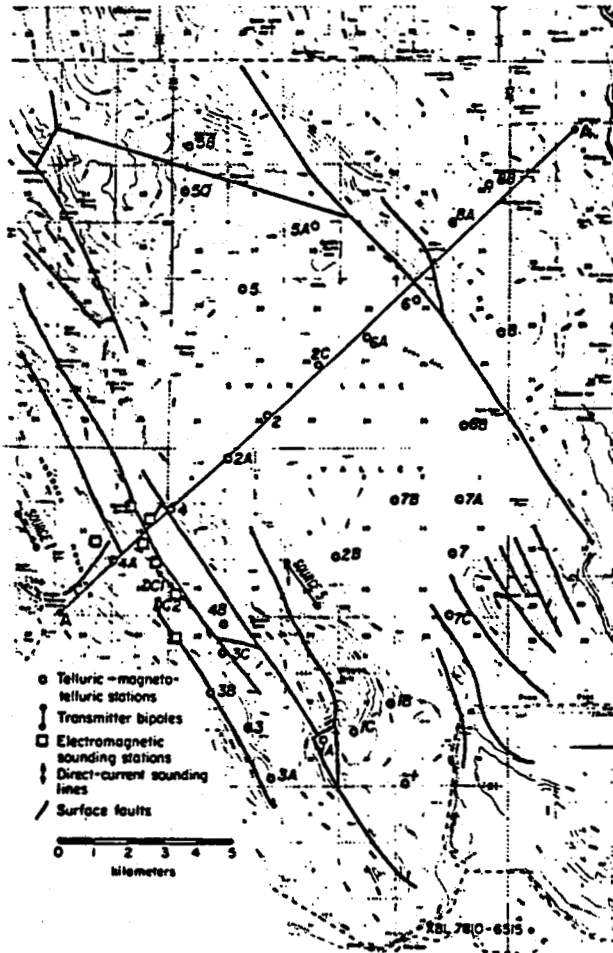fields were obtained at the base station with the
same number designation.
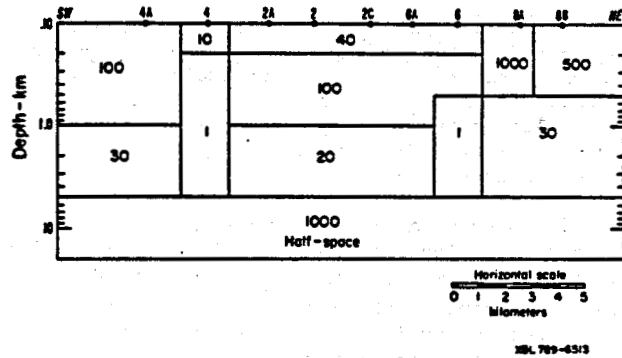

Figure 12   Initial two-dimensional model fit to
             the line of MT stations along line A-A',
             Swan Lake Valley area, Klamath County,
             Oregon.

For example, a comparison of the TE modes in
Figures 13 and 14 shows that we were unable to
obtain a good match between observed and calculated
pseudo-sections. The poorest match occurs in the
vicinity of telluric stations 8A and 8B which lie
on the Swan Lake rim, the up-thrown side of a fault
block elevated 500 m above Swan Lake Valley. While
there could be various reasons why we were unable
to fit the data, we surmised that the lack of three-
component magnetic information at these two stations
could have resulted in a mis-identification of which
of the two principal resistivity directions is
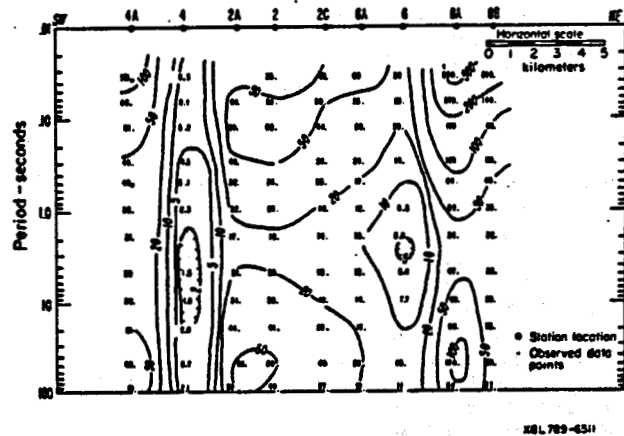associated with the TE mode.

Figure 11   Magnetotelluric stations in the
             Swan Lake Valley area, Klamath County,
             Oregon.

Figure 13   Measured TE mode apparent resistivity
             pseudo-section for line A-A', Swan Lake
             Valley, Klamath County, Oregon.

A 2-D fit to the data via forward modeling
yielded the resistivity model in Figure 12. We
were neither happy with nor confident in this
model because, despite repeated attempts to obtain
a better fit between observed and calculated
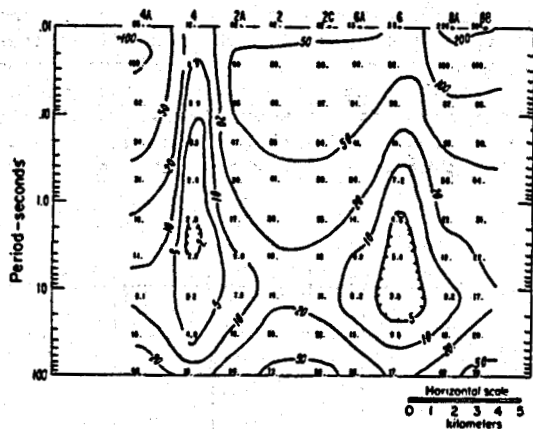pseudo-sections, we were unable to do so.

8

Figure 14. Calculated TE mode apparent resistivity pseudo-section (line A-A') for model shown in Figure 12.

There was also some doubt as to the proper mode identification at Station 4. We therefore interchanged the presumed TE and TM sounding data at stations 4, 8A, and 8B, to obtain the pseudo-section in Figure 15.
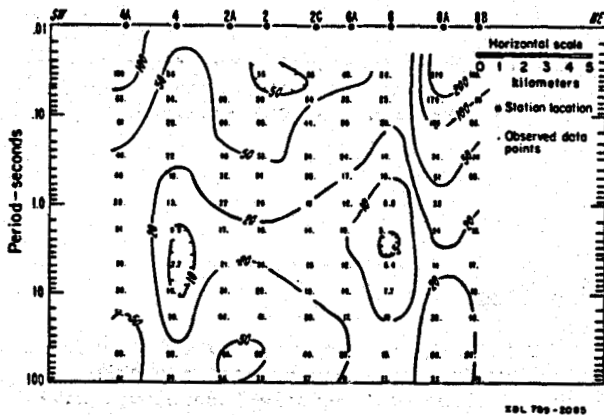

Figure 15 Measured TE mode apparent resisitvity pseudo-section (line A-A') after presumed TE and TM apparent resistiv-ities were interchanged at stations 4, 8A, and 8B.

Following the same modeling procedure as before, we then derived a new 2-D model (Figure 16) for which the calculated pseudo-section (Figure 17) shows a much better fit to the "observed" pseudo-section. The new model also reveals some detail absent in the first model; e.g., the conductive zone (6Ω m) at 1.0 to 1.5 km depth beneath the valley and the presence of a deeper crustal conductive zone (3 Ωm) at a depth of 20 km. The latter zone was later confirmed by results of the second survey, a regional MT survey across the Klamath graben, along a line passing over the valley.
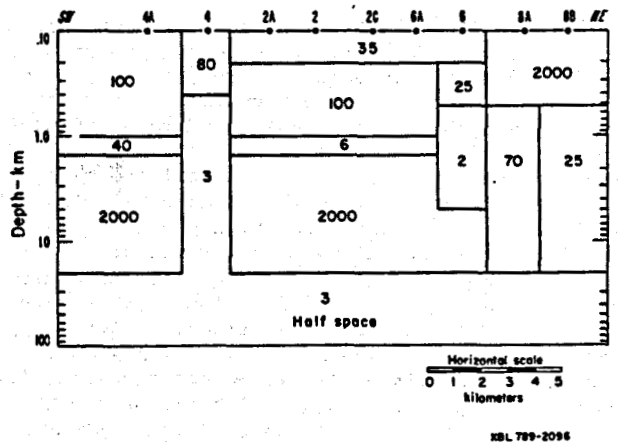

Figure 16 Revised two-dimensional model fit to the MT stations along line A-A' after inter-changing modes at stations 4, 8A, and 8B.
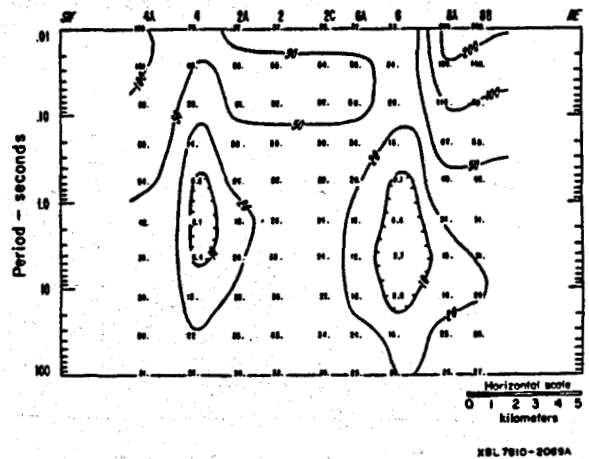

Figure 17 Calculated TE mode apparent resistivity pseudo-section (line A-A') for the revised two-dimensional model shown in Figure 16.

Despite the better fit, we are not totally confident in the revised model and there may yet remain errors, particular near the Swan Lake Rim. For example, as we made no topographic correction and our assumption regarding structural two-dimensionality is open to question, the conductive zone (2 Ω m) adjacent to the normal fault may be, in part, an artifact of interpretation. To resolve this question, additional MT stations supported by drilling or other geophysical methods would be necessary.

It should be clear, however, from this example, that considerable structural detail will be resolved if the station density is high. Narrow structures, such as the graben beneath station 4 (Meadow Lake Valley), can be resolved well. As the station separation is increased from 2 to 12 km, as the next example shows, the details are lost and the risk of spatial aliasing grows.

9

Figure 18 shows the locations of base (B) and remote (R) station pairs occupied by LBL for a remote magnetic reference MT survey along a line extending from the Siskyou Mountains, across the Cascades and the Klamath Basin, and terminating in the Basin and Range province near Bly, Oregon. The Swan Lake Valley occupies the central position of the area between stations B7 (Klamath Falls) and B8 (Yonna). The principal resistivity directions were found via the standard tensor rotation process, and the 90° ambiguity as to which direction can be taken as the regional geologic strike areas was resolved by choosing the direction closest to that for which T_y (equation (3)) is a maximum. This helped associate the two apparent resistivity soundings, $\rho_{xy}(\omega)$ or $\rho_{yx}(\omega)$, with either the TE or TM mode. The two sets of observed data, plotted in pseudo-section form, were jointly interpreted by means of a forward 2-D modeling algorithm. Data from Station 2A of the Swan Lake MT survey were included in the analysis to provide an additional sounding. It may be seen from Figure 15 that the specific choice of Station 2A, rather than another station in the valley (2 or 2C), imposes some bias on the interpretation, although the differences are slight.
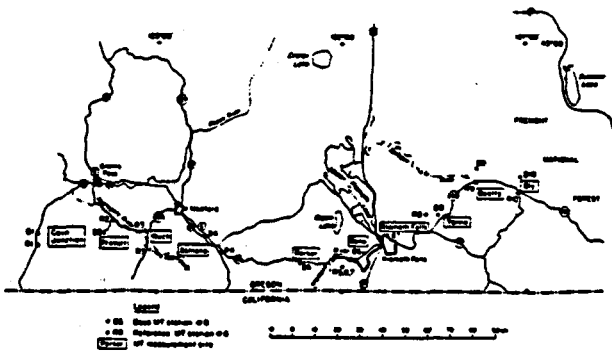

Figure 18 Location map of regional MT stations of a remote magnetic reference MT survey across the Klamath Basin, Oregon.

Figure 19 shows the resulting 2-D interpretation of the regional MT survey. Because this survey and the earlier Swan Lake Valley survey covered slightly different frequency bands, it is inappropriate to make a point-by-point detailed comparison of the two sets of results. However, it may be seen that both surveys discerned certain common features; e.g., (a) the low resistivity zone (4.3 Ωm) that occurs at a depth of 15-18 km beneath the basin, and (b) the high resistivity surface zone (610 Ωm) west of the Swan Lake Valley. On the other hand, important narrow 2-D features such as the Meadow Lake graben structure and perhaps the conductive zone adjacent to the Swan Lake Rim, both on the order of 1 km wide, cannot be resolved. However, we know from 2-D model studies that the presence of such structures may perturb the fields observed at stations 5 to 10 km away. Because the

effects of such inhomogeneities are small, they may not be readily suspected. The resulting interpretation will suffer from an indeterminant component of spatial aliasing which may manifest itself in the poorness of fit between observed and calculated pseudo-sections and large confidence limits calculated for certain resistivity units in the model.
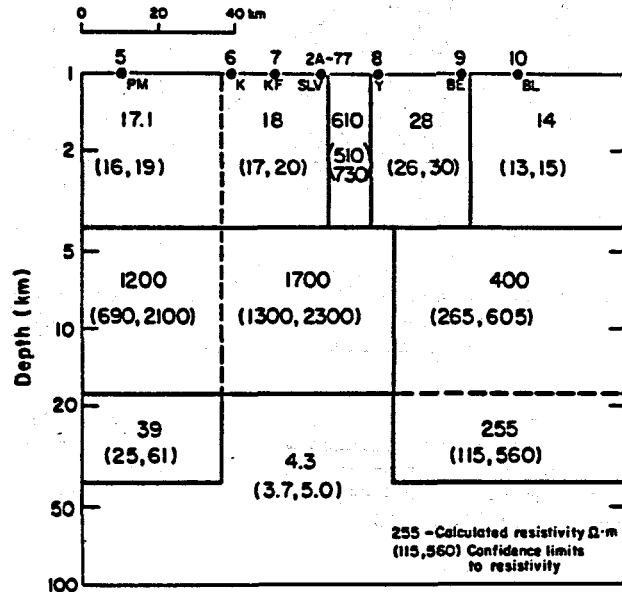
Figure 19 Two-dimensional model fitted to the regional MT survey between the Parker (PM) and Bly (BL) stations.

REFERENCES

Bostick, F.X., Jr., 1977, A Simple Almost Exact Method of MT Analysis in Workshop on Electrical Methods in Geothermal Exploration, University of Utah, Department of Geology and Geophysics, Salt Lake City, p. 175-177.

Cagnaird, L., 1953, Basic Theory of the Magnetotelluric method in geophysical prospecting: Geophysics, v. 18, p. 605.

Clarke, J., 1977, Superconducting Quantum Interference Devices for Low Frequency Measurements in Superconductor Applications: SQUIDs and Machines, B.B. Schwartz and S. Foner, editors, Plenum, New York, p. 67-124.

Clarke, J., 1980, Advances in SQUID Magnetometers, IEEE Transactions on Electron Devices, v.ED-27, p. 1896-1908.

Clarke, J., Goubau, W.M., and Ketchen, M.B., 1976, Tunnel Junction dc SQUID: Fabrication, Operation, and Performance, J. Low Temp. Phys., v.25, p. 99-144.

Coen, S., 1980, Direct Inversion of Two-Dimensional Magnetotelluric Data (abstract): Society of Exploration Geophysicists Annual Meeting, Houston.

Gamble, T.D., Goubau, W.M., and Clarke, J., 1979a, Magnetotellurics with a Remote Magnetic Reference, Geophysics, v.44, p. 53-68.

Gamble, T.D., Goubau, W.M., and Clarke, J., 1979b, Error Analysis for Remote Reference Magnetotellurics, Geophysics, v.44, p. 959-968.

Hermance, J.F., and Thayer R.E., 1976, The Telluric-Magnetotelluric Method, Geophysics, v.40, p. 664-668.

Hermance, J.F., Thayer, R., and Bjornsson, A., 1975, The Telluric-Magnetotelluric Method in the Regional Assessment of Geothermal Potential, Proceedings, Second U.N. Symposium on the Development and Use of Geothermal Resources, v.2, p. 1037-1047.

Hohmann, G.W., and Ting, S.C., 1978, Three-Dimensional Magnetotelluric Modeling, University of Utah, U.S. Department of Energy Report.

Jupp, D.L.B., and Vozoff, K., 1977, Two-Dimensional Magnetotelluric Inversion, Geoph. Jour. Royal Astron. Soc., v.50, n.2, p. 333-352.

Koch, R.H., and Clarke, J., 1979, Small Area Tunnel Junction dc SQUID, Bull. Am. Pys. Soc., v.24, p. 264.

Koch, R.H., Van Harlingen, D.J., and Clarke, J., 1981, Quantum Noise Theory for the dc SQUID, to be published in Applied Physics Letters.

Lee, K.H., and Morrison, H.F., 1980, A Solution for TM Mode Plane Waves Incident on a Two-Dimensional Inhomogeneity, Lawrence Berkeley Laboratory, Berkeley, Technical Report LBL-10649, 52 p.

Lee, K.H., Pridmore, D.F., and Morrison, H.F., 1980, A Hybrid 3D Electromagnetic Modeling Scheme, Lawrence Berkeley Laboratory, LBL-10378, 30 p. (submitted to Geophysics).

Oldenburg, D.W., 1979, One-Dimensional Inversion of Natural Source Magnetotelluric Observations, Geophysics, v.44, p. 1218-1244.

Pridmore, D.F., 1978, Three-Dimensional Modeling of Electrical and Electromagnetic Data Using the Finite Element Method, Ph. D. Dissertation, University of Utah.

Ryu, J., 1971, Low Frequency Electromagnetic Scattering, Ph.D. Thesis, University of California, Berkeley.

Stark, M., Goldstein, N.E., Wollenberg, H.A., 1980, Geothermal Exploration Assessment and Interpretation Upper Klamath Lake Area, Klamath Basin, Oregon, Lawrence Berkeley Laboratory, Berkeley, Technical Report LBL-10140, 84 p.

Stark, M., Goldstein, N., Wollenberg, H., Strisower, B., Hege, H., and Wilt, M., 1979, Geothermal Exploration Assessment and Interpretation, Klamath Basin, Oregon - Swan Lake and Klamath Hills Area, Lawrence Berkeley Laboratory, Berkeley, Technical Report LBL-8186, 75 p.

Swift, C.M., 1971, Theoretical Magnetotelluric and Turam Response from Two-Dimensional Inhomogeneities, Geophysics, v.36, p. 38-52.

Tesche, C.D., and Clarke, J., 1977, dc SQUID: Noise and Optimization, J. Low Temp. Phys., v.29, p 301-331.

Voss, R.F., Laibowitz, R.B., and Broers, A.N., 1980a, private communication.

Voss, R.F., Laibowitz, R.B., Raider, S.I., and Clarke, J., 1980b, All-Nb Low Noise dc SQUID with 1µm-Tunnel Junctions, J. Appl. Phys., v.51, p. 2306-2309.

Vozoff, K., 1972, The Magnetotelluric Method in the Exploration of Sedimentary Basins, Geophysics, v.37, p 98-141.

Weidelt, P., 1972, The Inverse Problem of Geomagnetic Induction, Zeitschrift fur Geophysik, v.38, p. 257-289.